ASTRONOMY & ASTROPHYSICS
SUPPLEMENT SERIES

Astron. Astrophys. Suppl. Ser. **142**, 65–72 (2000)

1.65 μm (H-band) surface photometry of galaxies

III. observations of 558 galaxies with the TIRGO 1.5 m telescope⋆

G. Gavazzi[1], P. Franzetti[1], M. Scodeggio[2], A. Boselli[3], D. Pierini[4], C. Baffa[5], F. Lisi[5], and L.K. Hunt[6]

[1] Università degli Studi di Milano - Bicocca, P.zza dell'Ateneo Nuovo 1, I-20126 Milano, Italy
[2] European Southern Observatory, Karl-Schwarzschild-Str. 2, D-85748 Garching bei München, Germany
[3] Laboratoire d'Astronomie Spatiale, Traverse du Siphon, F-13376 Marseille Cedex 12, France
[4] MPI für Kernphysik, postfach 103980, D-69117 Heidelberg, Germany
[5] Osservatorio Astrofisico di Arcetri, L.go E. Fermi 5, I-50125 Firenze, Italy
[6] C.A.I.S.M.I., L.go E. Fermi 5, I-50125 Firenze, Italy

Received October 5; accepted November 23, 1999

Abstract. We present near-infrared H-band (1.65 μm) surface photometry of 558 galaxies in the Coma Supercluster and in the Virgo cluster. This data set, obtained with the Arcetri NICMOS3 camera ARNICA mounted on the Gornergrat Infrared Telescope, is aimed at complementing, with observations of mostly early-type objects, our NIR survey of spiral galaxies in these regions, presented in previous papers of this series. Magnitudes at the optical radius, total magnitudes, isophotal radii and light concentration indices are derived. We confirm the existence of a positive correlation between the near-infrared concentration index and the galaxy H-band luminosity[1].

Key words: galaxies: fundamental parameters; galaxies: photometry; infrared: galaxies

1. Introduction

Over the last ten years or so, the advent of large format near-infrared (NIR) detectors has made images at wavelengths longer than 1 μm relatively easy to obtain. New infrared cameras based on these detectors make it straightforward to study statistically significant samples of galaxies in the NIR (see e.g. de Jong & van der Kruit 1994). The NIR wavelengths constitute the spectral region best adapted to studies of the quiescent stellar component of galaxies, since they trace mass better than do optical bands, being less contaminated by the low M/L products of recent episodes of star formation. The NIR spectral region is also relatively free of effects of dust, as extinction at 1.65 μm is more than seven times lower than in the B band (e.g., Landini et al. 1984). On the negative side, the sky brightness can be as much as ten magnitudes brighter than in the visible; thus more sophisticated and time-consuming observing and data reduction techniques are required.

Since 1993 we have used NIR arrays extensively to obtain images in the H bandpass of galaxies. The observing samples were selected by choosing members of the Virgo, Coma and A1367 clusters. In addition, we selected a significant population of galaxies in the portion of the "Great Wall" which lies in the bridge between Coma and A1367. These latter objects can be considered isolated and will be used as a control sample for environmental studies.

Our previous papers concentrated on spiral galaxies. About 160 such objects observed with the Calar Alto 2.2 m telescope were reported in Gavazzi et al. (1996c; Paper I); another 300, observed similarly with the TIRGO 1.5 m telescope, are given in Gavazzi et al. (1996b; Paper II); and another 102 Virgo galaxies are reported in Boselli et al. (1997; B97). More Calar Alto observations of 170 galaxies in the Virgo cluster are given in Boselli et al. (2000, Paper IV). In this paper, we present 1.65 μm (H-band) surface brightness measurements, obtained in 1997 at TIRGO equipped with the Arcetri NIR camera ARNICA, of 558 galaxies which are primarily of early-type (E-S0-S0a). We also provide several repeated measurements of late-type objects with previously unreliable photometry. Section 2 of the present paper describes

Send offprint requests to: G. Gavazzi

⋆ Based on observations taken at TIRGO (Gornergrat, Switzerland). TIRGO is operated by CAISMI-CNR, Arcetri, Firenze, Italy.

[1] Tables 1 and 2 are only available in electronic form at the CDS via anonymous ftp to cdsarc.u-strasbg.fr (130.79.128.5) or via http://cdsweb.u-strasbg.fr/Abstract.html

the current sample, and the observations are outlined in Sect. 3. Image analysis strategies are discussed in Sect. 4. Preliminary results are given in Sect. 5 and summarized in Sect. 6. Profile decompositions using combinations of exponential profiles and de Vaucouleurs laws of the present data and of those obtained similarly (Papers I, II, IV and B97) will be given in a forthcoming paper (Paper V of this series, Gavazzi et al. 1999a).

2. Sample selection

We report on the NIR H band observations of 558 optically-selected galaxies, for the most part (457) of early-type morphology, found in the regions of the Coma Supercluster and of the Virgo cluster. There are 383 early-type galaxies in the CGCG catalogue ($m_{\rm p} \leq 15.7$) (Zwicky et al. 1961-68) that are members of the Coma supercluster ($18^{\rm o} \leq \delta \leq 32^{\rm o}$; $11.5^{\rm h} \leq \alpha \leq 13.5^{\rm h}$), according to Gavazzi et al. (1999), i.e. with $5000 < V < 8000$ km s^{-1}. Of these, we have observed 372 objects, which constitute 97% of the designated sample.

We also observed 81 of the 98 early-type galaxies brighter than $m_{\rm p}$=14.0 listed in the VCC catalogue (Binggeli et al. 1985) which are bona-fide members of the Virgo cluster. Thus we have observed 83% of the giant early-type galaxies in Virgo.

The remaining 101 observations of spiral galaxies given here do not form a complete sample in any sense. However, they are necessary to define a complete data set. When combined with data published in Papers I and II (both of which were devoted to observations of spiral galaxies) Paper IV of this series and B97 (which contains mainly measurements of spiral galaxies in Virgo), the NIR survey presented in this series of papers represents a complete, optically selected sample of galaxies, which will be analyzed in future papers.

The first 9 columns of Table 1 give the optical parameters of the 558 galaxies studied in the present work as follows:
Column 1: CGCG (Zwicky et al. 1961-68) or VCC (Binggeli et al. 1985) denomination.
Column 2: NGC/IC names.
Columns 3, 4: adopted (1950) celestial coordinates, measured by us or taken from NED[2], with few arcsec uncertainty.
Column 5: "aggregation" parameter. This parameter defines the membership to a group/cluster/supercluster: CSisol, CSpairs, CSgroups indicate members of the Coma Supercluster ($5000 < V < 8000$ km s^{-1}); CSforeg means objects in the foreground of the Coma Supercluster ($V < 5000$ km s^{-1}) and CSbackg means objects in the background of the Coma Supercluster ($V > 8000$ km s^{-1}). Galaxies in the Virgo region are labelled following the membership criteria given by Binggeli et al. (1993): VCA, VCB, VCM, VCW, VCW′, VCSE, VCmem, are members to the cluster A or B, to the M, W, W′ or South-East clouds or are not better specified members to the Virgo cluster respectively. NOVCC are galaxies taken from the CGCG in the outskirts of Virgo, but outside the area covered by the VCC. VCback are galaxies in the background of the Virgo cluster ($V > 3000$ km s^{-1}).
Column 6: photographic magnitude as given in the CGCG or in the VCC.
Columns 7, 8: for CGCG galaxies these are the major and minor optical diameters (a_{25}, b_{25}) (in arcmin) derived at the B band 25$^{\rm th}$ mag arcsec^{-2}, as explained in Gavazzi & Boselli (1996). These diameters are consistent with those given in the RC3. For VCC galaxies these are the diameters measured on the du Pont plates at the faintest detectable isophote, as listed in the VCC.
Column 9: morphological type.

[2] NASA-IPAC Extragalactic Databasa (NED) is operated by the Jet Propulsion Laboratory, California Institute of Technology, under contract with NASA.

3. Observations

The observations reported in this paper were acquired with the 1.5 m, f/20 TIRGO telescope from March 13 to April 13, 1997, when 32 nights were allocated to the present project. Only 22/32 nights were useful, 16 of which were entirely or partly photometric. The seeing ranged from 1.5 to 3.5 arcsec (FWHM) with a mean of 2.4 arcsec, as shown in Fig. 1. These seeing conditions are mostly due to the large pixels ($\sim$1 arcsec) of ARNICA at TIRGO, and as such represent a necessary disadvantage, because they also provide the large field-of-view (4.1×4.1 arcmin^2) fundamental for our observations.

The folded Cassegrain focus of the telescope is equipped with the Arcetri NIR camera, ARNICA, which relies on a 256^2 NICMOS3 array detector (Lisi et al. 1993; Lisi et al. 1996; Hunt et al. 1996). With a pixel size of 0.97 arcsec, the field-of-view is 4.1×4.1 arcmin^2. Obtaining a satisfactory background subtraction is the main difficulty of NIR observations. At 1.65 μm, the sky brightness at the Gornergrat is $\approx$13.0 − 13.5 mag arcsec^{-2}, and varies on time scales comparable with the typical duration of an observation (e.g., Wainscoat & Cowie 1992). To achieve a brightness limit 8 mag arcsec^{-2} fainter than the sky requires an image in which the deviations from flatness do not exceed 0.06%. Thus, data acquisition techniques must be able to monitor the sky fluctuations and data reduction must take these into account.

To this end, we used two types of pointing sequences, or "mosaics", according to the size of the galaxy. Galaxies with an optical diameter $\geq$ 1 arcmin were observed using a sequence in which half of the time is devoted to the target, and half to the surrounding sky (hereafter denoted as

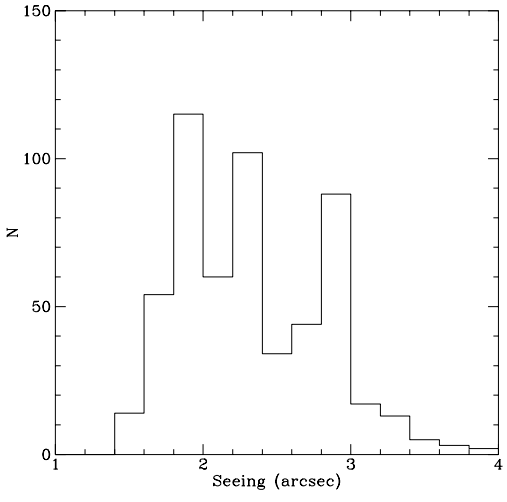

Fig. 1. The seeing distribution

a type "A" mosaic)[3]. Typically eight on-source pointings were alternated with eight on the sky, positioned along a circular path around the galaxy and offset by 4 arcmin from the source position. The on-source positions were "dithered" by 10 arcsec in order to facilitate the elimination of bad pixels. To save telescope time, small galaxies (with an optical diameter < 1 arcmin were observed with a pointing sequence consisting of nine pointings along a circular path and displaced from one another by 1 arcmin such that the target galaxy is always in the field (hereafter denoted as a type "B" mosaic).

On-chip integration times were set to 6 s to avoid saturation but to ensure background-limited performance. Total integration times on-source were typically 400 s and ranged from 150 to 950 s.

Table 1 gives the parameters relevant to the NIR observations as follows:
Column 10: number of frames $N_{\rm f}$ combined to form the final image (depending on the adopted mosaic).
Column 11: number of elementary observations (coadds) $N_{\rm c}$. The total integration time (in seconds) is the product of the number of coadds $N_{\rm c}$ times the number of combined frames $N_{\rm f}$ times the on-chip integration time $t_{\rm int}$ which was set to 6 s.
Column 12: seeing (in pixels, with 0.97 arcsec per pixel).
Column 13: adopted zero point (mag/s).
Columns 14-17: observing dates (day-month-1997).

[3] Sketches of the "mosaics" used can be found in Fig. 2 of B97.

3.1. Photometric calibration

Observations of the standard stars HD 84800 (H = 7.53 mag) and HD 129653 (H = 6.92 mag) from Elias et al. (1982) were taken hourly throughout the nights for calibration purposes. The calibration stars were observed with a third pointing sequence (mosaic type "C") which consisted of five positions, starting with the star near the center of the array, followed by positioning the star in each of the four quadrants of the array. The telescope was defocussed to avoid saturation. During the photometric nights (i.e. those of march 20, 21, 25, 27, 29, 31 and of April 1, 2, 6, 7 and 13) the typical uncertainty in the nightly calibration is 0.05 mag. Those nights were mostly used to observe galaxies with unknown H band photometry.

In the remaining non-photometric or marginally photometric nights we did not rely on the photometric calibration; instead we conservatively observed only those galaxies with aperture photometry available from the literature. For these galaxies the calibration was derived from the "virtual aperture photometry" (see Sect. 4.1 below).

Several (108) galaxies were observed in more than one night (see Cols. 14-17 in Table 1). This was done either to check the photometric consistency, because some observations were taken in non-photometric conditions, or, if the objects were fainter than average, to obtain a longer integration. For these objects we obtained an average frame by combining the various sets of observations, and using the zero point from the frame(s) taken under photometric conditions.

3.2. Data reduction procedures

Since dome exposures cannot be obtained at TIRGO due to the vicinity of the telescope secondary ring to the dome, the multiplicative correction for the system response, or flat-field (FF), was derived daily from the observations. Many tens (typically 30 to 40) sky frames taken in similar conditions throughout the night were combined with a median filter. The combined frame, normalized to its median counts was used as the flat-field frame.

The reduction procedure varied according to the type of mosaic. For type "A" mosaics, the (usually eight) sky exposures were combined with a median algorithm to form a median sky. For type "B" and "C" mosaics, the median sky was determined by combining all the frames in the pointing sequence. The median algorithm is necessary to remove unwanted star and galaxy images in the median sky frames. The median sky was first normalized to its median, then multiplied by the median counts of the individual target frames. Finally this rescaled frame was subtracted from each of the target observations. Such a procedure accounts for temporal variations in the sky level which are on the order of 5% during a pointing sequence,

Table 1. The program galaxies. This is a one page sample. The entire table containing 558 entries is only available in electronic format

Galaxy	NGC/IC	$R.A.1950$	$Dec.$	Agg	m_p	a	b	$type$	N_f	N_c	$Seeing$	Zp	$Date1$	$Date2$	$Date3$	$Date4$	H_{B25}	H^c_{B25}	H_T	$r_H(20.5)$	C_{31}
		$h\ m\ s$	$^o\ '\ "$		mag	$arcmin$	$arcmin$				pix	$mag\ s^{-1}$	dd/mm	dd/mm	dd/mm	dd/mm	mag	mag	mag	$arcsec$	
(1)	(2)	(3)	(4)	(5)	(6)	(7)	(8)	(9)	(10)	(11)	(12)	(13)	(14)	(15)	(16)	(17)	(18)	(19)	(20)	(21)	(22)
VC0049	4168	120943.50	132905.0	VCM	12.21	1.94	1.54	E	6	8	2.0	19.47	07/04				8.84	8.84	8.80	48.88	3.93
VC0094	4191	121116.80	072842.0	VCW	13.57	1.85	1.22	$S0a$	7	8	1.9	19.47	07/04				10.09	10.01	10.16	26.90	5.12
VC0122	4200	121210.80	122730.0	VCM	13.85	2.14	1.07	$S0$	6	8	2.6	19.25	09/04				10.23	10.23	10.30	29.69	5.04
VC0166	4215	121321.20	064045.0	VCW	13.12	2.69	0.72	$S0$	5	8	3.0	19.38	10/04				9.27	9.27	9.10	-1.00	6.10
VC0213	3094	121423.40	135413.0	VCA	14.26	1.12	0.86	$S-BCD$	8	8	1.9	19.46	02/04				11.54	11.54	11.52	15.42	2.94
VC0220	4233	121433.40	075403.0	VCW	12.97	3.39	1.07	$S0$	7	8	2.6	19.27	09/04				9.06	9.06	8.95	64.16	8.59
160250	4026	125757.50	281858.0	$Coma$	15.50	0.82	0.49	$S0$	7	8	2.2	19.45	31/03				11.88	11.88	11.54	13.86	4.92
160251	–	125811.00	282455.0	$Coma$	15.70	0.60	0.20	$S0a$	9	8	1.7	19.49	02/04				12.40	12.19	12.34	16.86	4.06
160253	4906	125815.10	281134.0	$Coma$	15.20	0.72	0.57	E	8	8	2.1	19.50	22/03				11.54	11.54	11.18	14.90	4.94
160254	4041	125816.49	281556.6	$Coma$	15.70	0.70	0.48	E	7	8	2.7	19.47	01/04				12.04	12.04	12.08	12.63	3.92
160255	4042	125818.20	281355.0	$Coma$	15.50	0.65	0.64	$S0$	7	8	2.7	19.47	01/04				11.42	11.42	11.09	16.68	5.81
160256	4045	125824.10	282135.0	$Coma$	15.10	0.84	0.64	E	7	8	2.5	19.50	22/03				11.22	11.22	11.24	14.36	3.61
160257	4907	125824.37	282537.8	$Coma$	14.60	1.13	1.08	Sa	8	8	1.9	19.45	31/03				10.72	10.71	10.68	28.38	3.79
160258	4908	125827.00	281842.0	$Coma$	14.90	0.92	0.68	E	30	6	2.5	19.50	15/03	24/03	25/03	31/03	10.93	10.93	10.60	21.36	5.52
160259	4051	125829.80	281640.0	$Coma$	14.80	1.49	0.98	E	29	6	2.5	19.52	16/03				10.78	10.78	10.64	24.44	4.40
160260	4911	125831.50	280336.0	$Coma$	13.70	1.89	1.50	Sa	7	8	1.7	19.48	23/03				10.06	10.02	10.28	28.17	2.75
161029	–	131912.70	263359.0	$CSbac$	15.70	0.40	0.30	E	9	8	2.0	19.49	02/04				12.37	12.37	12.22	11.36	3.25
161030	–	131920.69	313645.1	$CSfor$	14.80	1.40	0.60	$S0$	8	8	1.7	19.47	08/04				11.57	11.57	11.70	17.82	2.50
161034	–	131942.37	313222.9	$CSmul$	15.70	0.40	0.30	$S0$	16	8	2.6	19.47	04/04	06/04			12.07	12.07	12.06	12.03	2.54
161040	–	132102.70	264819.3	$CSiso$	15.60	0.74	0.40	Sc	9	8	2.1	19.49	02/04				12.85	12.74	12.73	11.11	3.13
161041	–	132122.30	315421.0	$CSfor$	15.50	0.80	0.50	$S..$	8	8	2.0	19.30	11/04				12.27	12.27	11.92	16.31	4.18
161042	5127	132125.80	314934.0	$CSfor$	13.90	2.30	1.70	E	6	8	1.9	19.43	11/04				9.77	9.77	9.84	33.19	4.28
161043	5131	132137.37	311453.4	$CSiso$	14.40	2.20	0.44	Sa	16	6	2.9	19.49	17/03	25/03			10.32	10.02	10.19	43.41	6.95
161044	–	132156.69	313620.0	$CSfor$	15.30	1.50	0.25	Sc	7	8	2.0	19.45	14/04				11.52	11.18	11.34	36.27	3.76
161046	4241	132224.80	265953.0	$CSiso$	15.50	0.60	0.60	E	8	8	2.7	19.46	30/03				11.83	11.83	11.46	14.83	4.39
161047	–	132234.40	264325.0	$CSiso$	15.60	0.80	0.35	E	9	8	2.6	19.47	01/04				11.65	11.65	11.38	16.15	7.54
161050	–	132402.10	315731.0	$CSbac$	15.60	0.50	0.30	E	17	6	3.0	19.49	21/03	01/04			12.38	12.38	12.32	9.97	3.30
161052	–	132430.00	265101.5	$CSiso$	15.10	0.30	0.30	$I-Pec$	9	8	3.0	19.46	30/03				12.42	12.42	12.24	9.19	3.68
161066	–	132714.00	264006.0	$CSiso$	15.70	1.00	0.20	$S..$	18	8	2.8	19.48	31/03	06/04			12.18	11.87	11.88	19.12	3.43
161070	–	132748.19	313845.6	$CSiso$	15.00	1.00	0.90	$S0$	15	6	3.0	19.49	20/03	30/03			11.33	11.33	10.98	17.24	4.14
161071	–	132758.62	313530.3	$CSfor$	14.90	1.30	0.51	$I-Pec$	8	8	1.7	19.47	08/04				12.80	12.80	13.19	12.15	2.67
161075	–	132824.50	264643.0	$CSiso$	15.70	0.70	0.30	E	16	8	2.9	19.48	31/03	06/04			13.79	13.79	13.51	9.56	3.54

but introduces an additive offset which is subsequently removed (see below). The sky-subtracted target frames are then divided by the FF frame. Each of these corrected frames was then analyzed for low-spatial-frequency gradients, and if necessary, fitted with a two-dimensional 3 degree polynomial which was then subtracted. (We carefully checked that this procedure did not produce artificial features which could disturb the photometry of the target objects). If this process was not effective in removing the spatial gradients, the corresponding frames were rejected from further analysis. Finally, the corrected frames were registered using field stars and combined with a median filter which allows bad pixel removal. Foreground stars were eliminated by manual "editing" of the target frames. All image reduction and analysis was performed in the IRAF environment and relied on the STSDAS package[4].

We have assessed the quality of the final images both on small spatial scales, and over the entire array. All of the images are truly background limited, as the noise we measure is the same as that which we would theoretically expect from the statistical fluctuations in the sky background, according to Hunt & Mannucci (1998)

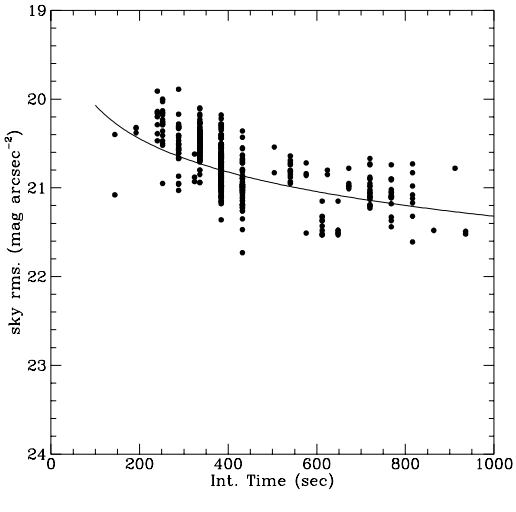

Fig. 2. The distribution of the sky rms as a function of integration time. The solid line is the prediction by Hunt & Mannucci (1998)

(see Fig. 2). The typical pixel to pixel fluctuations are ~ 21 mag arcsec^{-2} , i.e. $0.05-0.06\%$ of the sky.

4. Image analysis

4.1. H-band magnitudes from virtual aperture photometry

At the position of the galaxies' centers (determined by fitting a two-dimensional Gaussian to the galaxies) a

[4] IRAF is the Image Analysis and Reduction Facility made available to the astronomical community by the National Optical Astronomy Observatories, which are operated by AURA, Inc., under contract with the U.S. National Science Foundation. STSDAS is distributed by the Space Telescope Science Institute, which is operated by the Association of Universities for Research in Astronomy (AURA), Inc., under NASA contract NAS 5–26555.

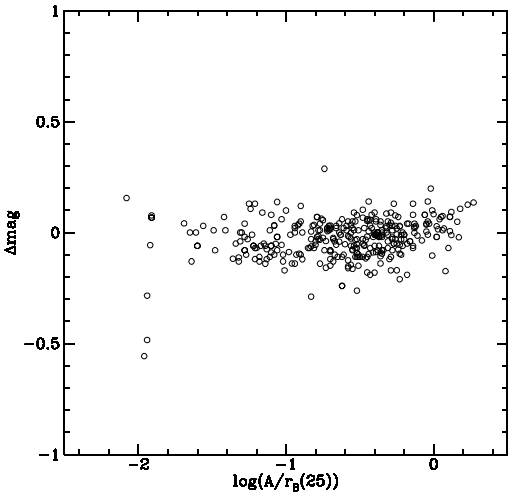

Fig. 3. The comparison between the present photometric measurements and those available from the literature as a function of the normalized aperture

growth curve was derived for each object by integrating the counts in concentric circular rings of increasing radii. The background was determined in a concentric object–free corona (where the contribution from contaminating stars is rejected by average sigma–clipping). The measurements taken through the individual "virtual circular apertures" are useful to compare with existing similarly taken measurements (e.g. Gezari et al. 1993) and for calibration purposes of future observations. They are given in Table 2 (available only in digital format) as follows:
Column 1: Galaxy denomination in the CGCG (Z) or VCC catalogues.
Column 2: aperture diameter in arcsec.
Column 3: logarithmic ratio of the adopted aperture diameter to the optical (a_{25}) diameter.
Column 4: integrated H magnitude within the aperture.

The photometry of 159 galaxies observed under photometric conditions has been checked against 187 published aperture photometry measurements (see Gezari et al. 1993). The comparison of our "virtual aperture" measurements with the reference photometry, taken through apertures consistent with ours, is given in Fig. 3. On the average we find:
$H_{\rm this\ work} - H_{\rm literature} = -0.026 \pm 0.095$ mag.

The most discrepant measurements are those taken through small apertures ($5 - 15$ arcsec), due to a combination of seeing effects and unaccurate galaxy centering. We estimate the overall photometric accuracy of our data, including systematic errors in the calibration, to be ≤ 0.1 mag.

Table 2. The "virtual aperture photometry". This is a one page sample. The entire table containing 6293 entries is only available in electronic format

Galaxy	*Ap.* arcsec	logAp/a_{25}	*H* mag
(1)	(2)	(3)	(4)
Z 97005	3.80	−1.15	15.31
Z 97005	5.80	−.97	14.58
Z 97005	7.70	−.85	14.09
Z 97005	9.60	−.75	13.78
Z 97005	11.50	−.67	13.52
Z 97005	15.40	−.54	13.15
Z 97005	16.70	−.51	13.05
Z 97005	19.20	−.45	12.92
Z 97005	22.50	−.38	12.80
Z 97005	26.90	−.30	12.67
Z 97005	30.70	−.25	12.61
Z 97005	34.60	−.19	12.56
Z 97005	38.40	−.15	12.53
Z 97011	3.80	−.80	14.67
Z 97011	5.80	−.62	14.04
Z 97011	7.70	−.49	13.67
Z 97011	9.60	−.40	13.43
Z 97011	11.50	−.32	13.26
Z 97011	15.40	−.19	13.09
Z 97011	16.70	−.16	13.05
Z 97011	19.20	−.10	13.01
Z 97011	22.50	−.03	12.97
Z 97011	26.90	.05	12.97
Z 97013	3.80	−1.10	16.29
Z 97013	5.80	−.92	15.61
Z 97013	7.70	−.79	15.21
Z 97013	9.60	−.70	14.96
Z 97013	11.50	−.62	14.76
Z 97013	15.40	−.49	14.58
Z 97013	16.70	−.46	14.53
Z 97013	19.20	−.40	14.53
Z 97013	22.50	−.33	14.51
Z 97021	3.80	−.98	12.59
Z 97021	5.80	−.79	12.12
Z 97021	7.70	−.67	11.87
Z 97021	9.60	−.57	11.71
Z 97021	11.50	−.50	11.58
Z 97021	15.40	−.37	11.41
Z 97021	16.70	−.33	11.36
Z 97021	19.20	−.27	11.29
Z 97021	22.50	−.20	11.21
Z 97021	27.10	−.12	11.13
Z 97021	31.50	−.06	11.07
Z 97021	34.90	−.01	11.02
Z 97021	38.40	.03	10.98

4.2. Isophotal radii, total magnitudes, and concentration indices

Our NIR observations available so far (including those given in Papers I, II and IV and in B97) were also analyzed using a more sophisticated approach than the one adopted here: 1) the surface brightness profiles were derived from azimuthally averaged elliptical isophotes with center, ellipticity and position angle taken as free parameters. 2) the surface brightness profiles were decomposed into combinations of exponential and de Vaucouleurs laws (or double exponential profiles) using a fitting algorithm. We prefer to postpone the discussion of these profile

decompositions to a forthcoming paper (Paper V of this series; some details of the decomposition procedures can be found in Scodeggio et al. 1998). However we wish to anticipate here a few results which depend on the fitting algorithms only as a tool necessary to extrapolate the measured photometry to infinity: i.e. to obtain total magnitudes, concentration indexes and also to derive isophotal radii at a given limiting surface brightness (20.5 mag arcsec^{-2}in this cse) when the observations do not reach such a limit.

Table 1 gives the H band measured parameters of the observed galaxies, as follows:
Column 18: $H_{\rm B25}$ magnitude obtained extrapolating the present photometric measurements to the optical diameter along circular apertures as in Gavazzi & Boselli (1996).
Column 19: $H^{\rm c}_{\rm B25}$ magnitude computed at the optical diameter (see Col. 18) corrected for galactic and internal extinction following Gavazzi & Boselli (1996). The adopted internal extinction correction is $\Delta m = -2.5\,D\,\log(b/a)$ where $D = 0.17$, as determined in Boselli & Gavazzi (1994).
Column 20: $H_{\rm T}$ total H magnitude extrapolated to infinity along either an exponential or a de Vaucouleurs $r^{1/4}$ law fitted to the outer parts of the observed radial surface brightness profiles (see Paper V for details).
Column 21: galaxy observed major ($r_H(20.5)$) radius (in arcsec) determined in the elliptical azimuthally–integrated profiles as the radius at which the surface brightness reaches 20.5 H–mag arcsec^{-2}. Galaxies which require a surface brightness extrapolation larger than 0.5 mag to reach the 20.5$^{\rm th}$ magnitude isophote are labelled -1.
Column 22: the model–independent concentration index C_{31}, as defined in de Vaucouleurs (1977), is the ratio between the radii that enclose 75% and 25% of the total light $H_{\rm T}$.

5. Results

Based on the observations presented in this work, which we reiterate does not comprise a complete sample, we derive the following preliminary results.

5.1. Radii $r_H(20.5)$

The isophotal radii in this work are derived at the 20.5 mag arcsec^{-2} H-band isophote, which represents a rather bright level, even for H-band measurements. For example in Papers I and II we were able to measure similar quantities one mag arcsec^{-2} fainter, i.e. up to 21.5 mag arcsec^{-2}. This is not due to lower signal-to-noise of the present data compared with the past data, but rather to the different method adopted for deriving the light profiles. In the previous papers the radial surface brightness profiles were derived by azimuthally integrating the counts in concentric elliptical coronae of fixed center and ellipticity up to indefinite radii. Here, instead, the center and ellipticity are kept as free parameters and the fitting is halted when the mean surface brightness within a given elliptical corona equals the corresponding rms. fluctuation. The drawback is that the new fitting routine halts at higher surface brightnesses than before. The lowest surface brightness reached in each image is given in Fig. 4 as a function of the integration time.

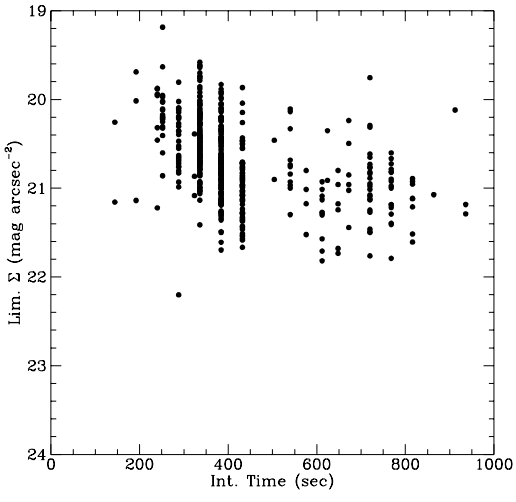

Fig. 4. The distribution of the lowest surface brightness reached in the outer light profiles, as a function of the exposure time

The comparison between the isophotal B band $r_B(25.0) = (a/2)_{25}(B)$ radii (Gavazzi & Boselli 1996) and the infrared $r_H(20.5)$ isophotal radii determined in this work is shown in Fig. 5. Apart from the curvature apparent at small radii, the data are consistent with $r_H(20.5) = 0.7\ r_B(25.0)$ between these two arbitrary isophotal levels.

This indicates that at the adopted isophotal level, the H observations cover a substantial fraction of the light, and are not restricted to the bulge. The relationship between optical and H-band isophotal radii is consistent with that expected from our limiting H surface brightness of 20.5 mag arcsec^{-2} and with the $B-H$ color of the outer portion of normal galaxies.

The curvature seen in Fig. 5 is only marginally an artefact of the seeing: the effect is reduced slightly by removing the objects observed in the worse seeing conditions. The deviation from linearity is not due to an overestimate of the H band radii, rather it reflects an underestimate of the B band diameter of small ($\leq$ 10 arcsec) early-type

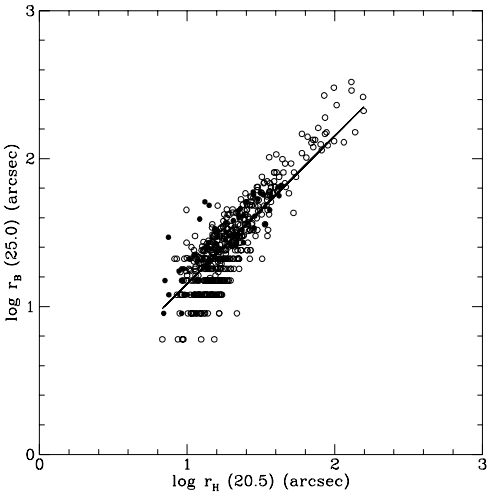

Fig. 5. The relation between the apparent major isophotal radius $r_H(20.5)$ as determined in the infrared (this work) and in the optical $r_B(25.0)$. E+S0 are plotted as open circles, S+Irr as filled circles. The solid line represents the relation $r_H(20.5) = 0.7\ r_B(25.0)$

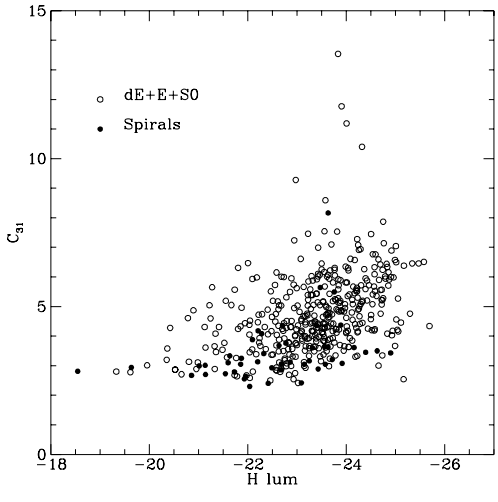

Fig. 6. The dependence of the near–infrared concentration index C_{31} on H band luminosity

galaxies which are intrinsically red (see Paper V for a more comprehensive discussion on this issue).

5.2. Magnitudes (H_T, H_{B25})

$H_{\rm B25}$ magnitudes listed in Col. 18 of Table 1 are obtained by extrapolating the circular aperture measurements to the optical $r_B(25.0)$ radius (as in Gavazzi & Boselli 1996). $H_{\rm T}$ mag instead are obtained by extrapolating to infinity the magnitude integrated along elliptical isophotes using combinations of exponential and de Vaucouleurs laws. As expected, $H_{\rm T}$ are brighter than $H_{\rm B25}$ by 0.10 ± 0.2 mag on average.

5.3. Concentration index (C_{31})

The concentration index C_{31} is a measure of the shape of light profiles in galaxies, independent of a bulge–disk decomposition. Values larger than $C_{31} > 2.8$ indicate the presence of substantial bulges.

We confirm the presence in our sample of a general correlation between C_{31} and the H band ($H_{\rm T}$ or $H_{\rm B25}$) luminosity (computed from the redshift distance). We find that C_{31} generally increases toward higher absolute magnitudes (Fig. 6). High C_{31} are found only among high luminosity systems, but the converse is not true: there are several high luminosity systems (namely late–type giant spirals) with no or little bulge ($C_{31} \sim 3$).

6. Summary

We have obtained images in the near-infrared H bandpass for an optical-magnitude-selected ($m_{\rm p} \leq 15.7$) sample of 558 nearby ($z < 0.02$) galaxies primarily of early-type, in the regions of Coma and Virgo. We derived H magnitudes at the optical radius, total H magnitudes, isophotal radii at the 20.5 mag arcsec^{-2} isophote, and the light concentration index C_{31}. As mentioned in the Introduction, the galaxies presented in this paper do not form by themselves a complete sample. Therefore we postpone the comprehensive analysis of the NIR properties of galaxies to forthcoming papers of this series. Paper V will report on the profile decomposition.

Acknowledgements. We wish to thank the TIRGO T.A.C. for the generous time allocation to this project and the TIRGO team for support during the observations. We thank A. Borriello, V. Calamai, B. Catinella, I. Randone, P. Ranfagni, M. Sozzi, P. Strambio for their assistance during the observations at TIRGO. A special thank to V. Gavriusev for software assistance at TIRGO.

References

Binggeli B., Sandage A., Tammann G., 1985, AJ 90, 1681
Binggeli B., Popescu C., Tammann G., 1993, A&AS 98, 275
Boselli A., Gavazzi G., 1994, A&A 283, 12
Boselli A., Tuffs R., Gavazzi G., Hippelein H., Pierini D., 1997, A&AS 121, 507 (B97)
Boselli A., Gavazzi G., Franzetti P., Pierini D., Scodeggio M., 2000, A&AS 142, 73 (Paper IV)
de Jong R., van der Kruit P., 1994, A&AS 106, 451

de Vaucouleurs G., 1977, in "Evolution of Galaxies and Stellar Populations", Larson R. & Tinsley B. (eds.). New Haven: Yale University Observatory, p. 43
Elias J., Frogel J., Matthews K., Neugebauer G., 1982, AJ 87, 1029
Gavazzi G., Boselli A., 1996, Ap. Lett. Comm 35, 1
Gavazzi G., Pierini D., Boselli A., Tuffs R., 1996c, A&AS 120, 489 (Paper I)
Gavazzi G., Pierini D., Baffa C., Lisi F., Hunt L., Boselli A., 1996b, A&AS 120, 521 (Paper II)
Gavazzi G., Pierini D., Boselli A., 1996a, A&A 312, 397
Gavazzi G., Carrasco L., Galli R., 1999, A&AS 136, 227
Gavazzi G., Franzetti P., Scodeggio M., Boselli A., Pierini D., 1999a, A&AS (in preparation) (Paper V)
Gezari D., Schmitz M., Pitts P., Mead J., 1993, Nasa Reference Publication, 1294
Hunt L., Lisi F., Testi L., Baffa C., Borelli S., Maiolino R., Moriondo G., Stanga R., 1996, A&AS 115, 181
Hunt L., Mannucci F., 1998, Arcetri Technical Report N. 2/98
Landini M., Natta A., Salinari P., Oliva E., Moorwood A., 1984, A&A 134, 284
Lisi F., Baffa C., Hunt L., 1993, SPIE 1495, 594
Lisi F., Baffa C., Bilotti V., et al., 1996, PASP 108, 364
Scodeggio M., Giovanelli R., Haynes M., 1998, AJ 116, 2728
Wainscoat R., Cowie L., 1992, AJ 103, 332
Zwicky F., Herzog E., Karpowicz M., Kowal C., Wild P., 1961-1968, "Catalogue of Galaxies and Clusters of Galaxies", Vol. 6, Pasadena, C.I.T.